Acta Astronautica 159 (2019) 385–396

Contents lists available at ScienceDirect

Acta Astronautica

journal homepage: www.elsevier.com/locate/actaastro

High-fidelity contingency trajectory design and analysis for NASA's near-earth asteroid (NEA) Scout solar sail Mission☆

James Pezent[a,*], Rohan Sood[a,c], Andrew Heaton[b,1]

[a] 245 7th Ave, Tuscaloosa, AL, 35401, USA
[b] NASA MSFC, Building 4600, Huntsville, AL, 35808, USA
[c] Assistant Professor of Aerospace Engineering and Mechanics, Astrodynamics and Space Research Laboratory, The University of Alabama, USA

ABSTRACT

Exploratory missions to investigate accessible Near Earth Asteroids (NEAs) can benefit from leveraging dynamics associated with a solar sail-based spacecraft. As a part of this effort, NEA Scout is a solar sail mission designed to propel a 6U CubeSat by harnessing solar radiation pressure from the Sun. The spacecraft will be launched as a secondary payload on NASA's Space Launch System (SLS) Exploration Mission One (EM-1). As the launch of EM-1 has recently been rescheduled for December 2019, alternative target NEAs are identified. Additionally, solar sail-based trajectories for the NEA Scout mission also need to be reevaluated. In this study, high-fidelity trajectories for the NEA Scout mission are investigated for varying launch dates under the assumption of the failure of a critical propulsive maneuver. Furthermore, feasible trajectory solutions are presented for multiple candidate asteroids.

1. Introduction

Recent developments in solar sail technology as an in-space propulsion system have expanded mission scenarios for scientific exploration. Solar sailing provides a unique opportunity to harness the solar radiation pressure (SRP) and leverage the dynamics to maneuver a sail-based spacecraft. Solar sailing was first successfully demonstrated by JAXA's Ikaros Spacecraft in 2010 [1]. NASA's Nano Sail D (2010) and the Planetary Society's Light Sail A (2015) have further increased confidence in sail technology [2,3]. The Near Earth Asteroid (NEA) Scout mission is a joint effort between NASA's Marshall Space Flight Center (MSFC) and Jet Propulsion Laboratory (JPL) to perform a close flyby and investigate a small Near Earth Asteroid (NEA). The NEA Scout spacecraft is equipped with an 86 m^2 solar sail as the primary means of propulsion to maneuver and reach the target destination. As a precursor to human missions to asteroids, NEA Scout delivers a cost-effective opportunity to study the asteroid and address NASA's Strategic Knowledge Gaps (SKGs) as identified by the Human Exploration and Operations Mission Directorate (HEOMD) [4,5].)

1.1. Spacecraft specifications

A 6U CubeSat, provided by JPL, forms the main bus of the 12 kg spacecraft and houses all propulsion, avionics, and survey equipment. A schematic illustrating the location of relevant components within the craft can be seen in Fig. 1(a). The 86 m^2 solar sail is constructed from an aluminized colorless polymer (CP-1) and is shown in Fig. 1(b) [6,7]. Four flexible, 6.8 m long booms are responsible for deploying the sail from the initial stowed position in the central 2U of the spacecraft bus [7]. Both the sail and the deployment mechanism are designed by MSFC and based on the technology developed for NASA's NANOSail-D and the Planetary Society's Lightsail-A [4,7]. Additional propulsion for detumbling and course correction capabilities is delivered by a cold gas thruster system providing 38 m/s of total ΔV. Attitude control is maintained via a combination of reaction wheels, active mass translator (AMT), and cold gas thrusters. The four reaction wheels, each providing 0.004 N-m of torque, are arranged in a pyramidal formation for redundancy, and perform the majority of roll, pitch, and yaw maneuvers [8]. The active mass translator adjusts the spacecraft's center of mass to center of pressure offset, aiding in maneuvering and momentum desaturation about the pitch and yaw axes. A ΔV of 5 m/s is also held in reserve to offload the excess momentum accumulated in NEA Scout's roll axis. The combined system is capable of angular rates of 0.04 deg/s about the pitch and yaw axis and 0.02 deg/s about the roll axis. NEA Scout's primary scientific instrument is an ECAM M − 50 narrow field-of-view camera provided by JPL. It is capable of high resolution imaging of the target NEA's surface. The camera, along with an on-board star tracker, will be used to optically navigate the spacecraft throughout the planned trajectory.

☆ A previous version was presented at the 2018 AIAA Scitech Forum (AIAA 2018-0199).

* Corresponding author. Student, Astrodynamics and Space Research Laboratory, The University of Alabama, USA.
E-mail address: jbpezent@crimson.ua.edu (J. Pezent).
[1] Senior Aerospace Engineer, EV/42, NASA Marshall Space Flight Center.

https://doi.org/10.1016/j.actaastro.2019.03.050
Received 9 October 2018; Received in revised form 4 February 2019; Accepted 16 March 2019
Available online 21 March 2019

Nomenclature

β_{ideal}	lightness parameter of ideal solar sail
$\vec{B}$	slack variables vector
$\vec{C}$	mission constraints vector
$\vec{F}$	dynamic constraints vector
$\vec{r}$	spacecraft position vector
$\dot{\vec{r}}$	spacecraft velocity vector
$\ddot{\vec{r}}$	spacecraft acceleration vector
$\vec{X}_i$	solar sail state vector
$\dot{\vec{X}}_i$	time derivative of solar sail state vector
$\vec{X}_L$	solar sail trajectory vector

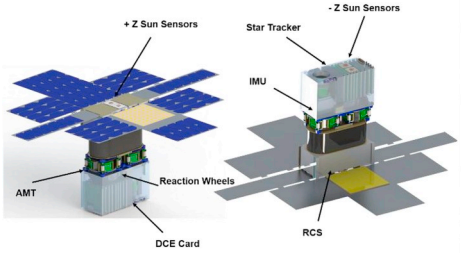

(a) The NEA Scout 6U CubeSat bus[8].

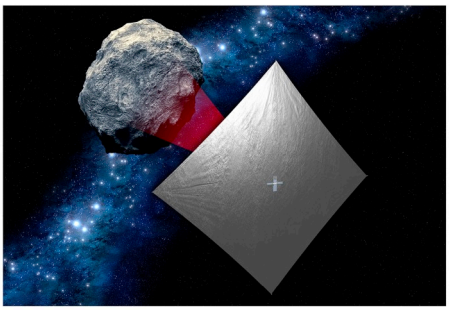

(b) An artist's rendition of NEA Scout surveying a target asteroid (1991 VG)[4].

Fig. 1. The NEA Scout spacecraft.

1.2. Mission plan

The current mission plan calls for NEA Scout to be launched as a secondary payload on Space Launch System's (SLS) inaugural flight, Exploration Mission One (EM-1), which will deliver NASA's Orion capsule on its maiden voyage to the Moon. Following EM-1's translunar injection burn and the Orion spacecraft's separation, NEA Scout will be ejected from the upper stage of the SLS. The cold gas thrusters will then expend 10 m/s of ΔV to detumble the rapidly spinning spacecraft and target a planned lunar flyby [9]. It will then spend roughly two weeks in the vicinity of the Moon awaiting for the precise opportunity to depart towards the target asteroid. The intervening time will be used to deploy the sail and calibrate communications equipment. At the conclusion of this phase, the cold gas thrusters will perform another small propulsive maneuver, placing the spacecraft on a trajectory towards its primary target. Thereafter, the spacecraft will be propelled primarily by solar sail, with 28 m/s of ΔV being held in reserve for any desirable corrective maneuvers. Upon arrival in the vicinity of the target, NEA Scout will perform a flyby at a velocity of less than 100 m/s relative to the asteroid from a distance of less than 2 km, and use its on-board camera to characterize the asteroid's shape, spectral type, and rotational properties [4,5]. However, there is a considerable interest in how the failure of the initial outbound trim maneuver and the subsequent lunar flyby will affect the mission's success.

2. Objectives

The goal of this investigation is to explore NEA Scout trajectory options in the event of initial trim maneuver failure following separation from EM-1. The time-critical nature of the maneuver and limited available ΔV budget would result in the spacecraft being unable to perform a series of lunar flybys stipulated by the nominal mission plan, and therefore, render the spacecraft incapable of precisely targeting the necessary departure trajectory. In the intervening time, NEA Scout will fly past the Moon and continue on an uncontrolled Earth-escape trajectory. The first major corrective actions can only be performed once the sail and communications equipment have been correctly deployed and calibrated. Thus, this study aims to design alternative trajectories that start at the J2000 state vector corresponding to the first opportunity for initial corrective action (ICA-state), and still fulfill NEA Scout's mission goals.

To achieve mission success, the contingency trajectories will need to satisfy the following criteria:

1. Perform a flyby of the target NEA from a distance of less than 2 km.
2. At the time of the flyby, the relative velocity should be less than 100 m/s.
3. The solar sail remains pointed within ± 50° of the Sun-sail line.
4. The spacecraft remains within 1 AU of the Earth.

Items 1 and 2 represent the low-speed flyby requirement and allow for thorough characterization of the target asteroid upon arrival. The pointing angle restriction ensures sufficient sun exposure for solar panels and prevents damage to the spacecraft's mission-critical star tracker. The final requirement is a result of NEA Scout's limited communications range with Earth-based ground stations. The high priority contingency scenario will first be analyzed for the now defunct October 7, 2018 launch date. The ICA-state was supplied by Marshall Space Flight Center and occurs 17 days after separation from EM-1 on October 24, 2018. The location of NEA Scout relative to the Earth and Moon in the Sun-Earth rotating frame 50 days after the time of the ICA-state, T, can be seen below in Fig. 2. Emphasis will be placed on computing and optimizing trajectories towards this launch date's primary target, asteroid 1991 VG.

Low-speed flyby trajectories to alternate targets will then be computed and compared to the baseline contingency trajectory to 1991 VG. In addition, a search and assessment of possible high speed flyby trajectories to both 1991 VG and alternate targets will also be performed. During the course of this study, EM-1 was delayed from October 7, 2018 to December of 2019, motivating a renewed assessment of contingency options. Information from the October 24, 2018 ICA-state will first be generalized to allow for preliminary analysis of an arbitrary EM-1 launch date. These assumptions will be used to construct new ICA-states for EM-1 launches in December of 2019. Based on the characteristics of the resulting initial states, a set of possible rendezvous targets will be selected. Contingency trajectories to the set of candidate asteroids will

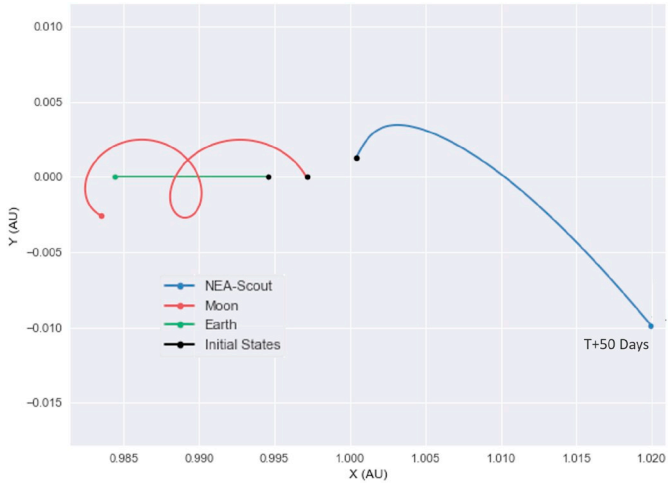

Fig. 2. Sun-Earth rotating frame view of NEA Scout's ICA-state propagated for 50 days from the time of the ICA-state, *T*.

then be computed and analyzed in a similar manner to the October 7, 2018 launch date.

3. Dynamical model

To accurately predict the behavior of NEA Scout under multiple gravitational and non-gravitational forces, a high fidelity dynamical model is developed. The system model is formulated in the international celestial reference frame (ICRF) and employs ephemeris data for the inertial time-dependent position history for all bodies under mutual gravitational influence. In addition, an ephemeris formulation for position-dependent solar radiation pressure is incorporated to model solar sail thrust.

3.1. n-body gravity model

While Keplerian and *3*-body gravity models offer excellent tools for preliminary analysis, a higher fidelity model is necessary to formulate a mission-operable trajectory. To this end, an *n*-body gravitational model leveraging NAAIF's C-Spice system and JPL's DE 431 planetary and lunar ephemeris is employed. The gravitational attractions of all relevant celestial bodies acting on the spacecraft may be succinctly stated by Equation (1),

$$\ddot{\vec{r}}_{gravity} = \sum_{i=1}^{n} \frac{\mu_i}{|\vec{r}_{ic}|^2} \hat{r}_{ic} \text{ with } \vec{r}_{ic} = \vec{r}_i - \vec{r}_c \tag{1}$$

where n represents the number of gravitationally attractive bodies under consideration, μ_i is the gravitational parameter of the i^{th} body, and $\vec{r}_{ic}$ represents the position vector directed towards the i^{th} body originating at the spacecraft, with $\hat{r}_{ic} = \vec{r}_{ic}/\|\vec{r}_{ic}\|$. Since NEA Scout will spend its entire relevant mission profile outside the sphere of influence of any planetary bodies under the contingency scenario, oblate gravitational effects are ignored and bodies are assumed to be point masses. The time-dependent position vectors of each body relative to the solar system's barycenter $\vec{r}_i$ are supplied by JPL's DE 431 ephemeris.

3.2. Solar radiation pressure model

Accurate modeling of the effects of solar radiation pressure (SRP) on NEA Scout's sail is critical to the construction of feasible trajectories. Without resorting to finite element analysis, an optical reflection model offers an excellent approximation of the solar sail's thrusting capability. The derivation of the model begins with that of a perfectly flat and reflecting surface at a distance of 1 AU from the Sun. In this form, all incident photons originating from the Sun are assumed to undergo perfectly elastic collisions with the sail's surface. Under these assumptions, the acceleration of the sail can be stated in Equation (2),

$$\vec{a}_{sail-1AU} = \frac{2P_0 A_{sail}}{m_{sail}} \cos^2 \alpha \, \hat{n} \tag{2}$$

where P_0 is the SRP at a distance of 1 AU, A_{sail} and m_{sail} are the area and mass of the sail-craft, $\hat{n}$ is the external unit vector normal to the sail surface in the inertial frame, α is the angle between the sail normal vector and Sun-sail line, and coefficient 2 arises from the perfect reflection assumption. Direction vector $\hat{n}$ itself is a function of cone angle α, clock angle γ, and the position of the sailcraft relative to the Sun. A new term β_{ideal} can now be introduced in Equation (3) as the ratio of the local acceleration due to the SRP, and the solar gravity at 1 AU.

$$\beta_{ideal} = \frac{2P_0 A_{sail} |\text{AU}|^2}{m_{sail}\, \mu_{sun}} \tag{3}$$

β_{ideal}, known as the lightness parameter, is the main performance metric of the sail and is constant with distance from the Sun, owing to the fact that both the SRP and the solar gravity are inverse square fields [10–12]. SRP acceleration at an arbitrary position can now be stated below. As in Equation (1), the Sun's position $\vec{r}_s$ is determined using the DE 431 ephemeris.

$$\ddot{\vec{r}}_{sail} = \frac{1}{2} \beta_{ideal} \frac{\mu_{sun}}{|\vec{r}_{sc}|^2} (2\cos^2 \alpha \, \hat{n}) \tag{4}$$

For NEA Scout, with a mass and sail area of 12 kg and 86 m^2, respectively, the ideal lightness parameter is 0.011. This model can then be modified to account for a non-ideal flat square sail in Equation (5) by considering the optical properties of the sail's reflective material [6,13].

$$\ddot{\vec{r}}_{sail} = \frac{1}{2} \beta_{ideal} \frac{\mu_{sun}}{|\vec{r}_{sc}|^2} \tag{5}$$

$$\left(\left(\left(1 + \tilde{r}s\right)\cos^2(\alpha) + B_f\left(1 - s\right)\tilde{r}\,\cos(\alpha)\right.\right.$$
$$\left.\left. + \left(1 - \tilde{r}\right)\left(\frac{e_f B_f - e_b B_b}{e_f + e_b}\right)\cos(\alpha)\right)\hat{n}\right.$$
$$+ ((1 - \tilde{r}s)\cos\alpha \sin\alpha)\,\hat{t})$$

Terms $\tilde{r}$ and s are the reflectivity and specular coefficients, respectively. B_f, B_b are the front and backside Lambertian coefficients of the sail, while e_f, e_b are the front and backside emissivity coefficients. These are based on updated testing done for the NEA Scout project in 2015 and are available in Table 1 [6].

The assumption of non-elastic photon collision also introduces a tangential component of SRP acceleration directed in the $\hat{t}$ direction that is not present in the ideal formulation. Its propulsive effects are small compared to that of the normal acceleration, but cannot be ignored if one is considering the effects of SRP torque upon the spacecraft. Such analysis is beyond the scope of this paper, but the propulsive effects are included and the sail is operated in an α envelope that will mitigate negative impact. The α and γ angles are not explicitly controlled via modeling of NEA Scout's attitude control systems. They are, instead, directly chosen in order to produce the desired orientation.

Table 1
NEA Scout optical coefficients.

$\tilde{r}$	s	B_f	B_b	e_f	e_b
0.91	0.89	0.79	0.67	0.025	0.27

4. Design strategy

4.1. Target and launch date analysis

When designing a contingency trajectory, it is important to first assess the viability of the primary target asteroid, as well as alternate targets that could potentially present better options. A survey of possible targets for NEA Scout based on the launch date of EM-1 can be seen in Fig. 3. The given times of flight (TOFs) are based on the assumption that NEA Scout is able to correctly perform the planned initial trim maneuver, and adequately target the necessary departure trajectory.

Trajectories for a subset of asteroids chosen for further investigation may be seen in Fig. 4. A 1 AU arc has been defined relative to the Earth indicating the communications barrier for the NEA Scout spacecraft. Each trajectory is shown from October 24, 2018 until the target's first crossing of this line.

Once the initial state when corrective maneuvers can be performed is defined (ICA-state), trajectory options can be directly explored. However, if the ICA-state is unknown or is subject to change, it is necessary to approximate the state in a manner that preserves the underlying contingency scenario. The following assumptions are made to modify an existing ICA-state to an arbitrary launch date.

1. EM-1's initial departure trajectory towards the Moon will be similar regardless of the launch date when viewed in the Earth-Moon rotating frame.
2. NEA Scout's separation and initial lunar flyby targeting maneuver will occur at roughly the same time relative to the launch date.
3. The new ICA-state will still occur the same number of days after separation from EM-1.

Based on these assumptions, the inertial ICA-state is first transformed into the Earth-Moon rotating frame. A new EM-1 launch date is chosen, and an additional 17 days are added to account for the time until the initial corrective action may be performed. The rotating frame ICA-state is then transformed back into the inertial frame relative to the Earth's position at the new epoch time. The approximated ICA-state may now be employed to perform preliminary analysis at the newly specified time.

For a given ICA-state (true or approximate), a simple heuristic approach is used to assess the feasibility of possible targets. First, a maximum allowable transfer time, T_{max}, is calculated from the elapsed time between NEA Scout's ICA-state and the target's first crossing of the 1 AU communications barrier.

A conservative estimate of the minimum possible transfer time, T_{min}, is obtained by considering that a relative inclination difference, θ_i, of roughly 0.2° at flyby will result in a relative velocity greater than the 100 m/s requirement. Therefore, T_{min} is the time necessary for NEA Scout to match the orbital plane of the target. This is calculated by considering the maximum possible rate of inclination change for a solar sail. Assuming a 2-body gravitational model, Lagrange's planetary equations can be solved to yield a closed form solution in the case of an ideal sail as seen in Equation (6) [14–16].

$$\Delta i = 88.2\,\beta_{ideal}\ \text{deg/orbit} \tag{6}$$

If it is assumed that NEA Scout has a β_{ideal} of 0.011 and remains at an average 1 AU distance from the Sun, it can be shown that $\Delta i_{avg} = .00265$ deg/day. T_{min} may then be attained by dividing the relative inclination between NEA Scout's initial transfer orbit and the target asteroid by Δi_{avg} as shown in Equation (7).

$$T_{min} = \theta_i \frac{1}{\Delta i_{avg}};\ \theta_i = acos\left(\frac{\vec{h}_{NEA} \bullet \vec{h}_{Targ}}{|\vec{h}_{NEA}||\vec{h}_{Targ}|}\right) \tag{7}$$

Terms $\vec{h}_{NEA}$ and $\vec{h}_{Targ}$ represent the specific angular momentum vectors of the spacecraft and target about the Sun in the ephemeris system. The proximity of these two times provides a quick indicator of NEA Scout's ability to successfully reach the target asteroid. If T_{min} exceeds T_{max}, it is fair to assume:

1. The relative velocity of a flyby occurring at any time before the target's crossing of the communications barrier will be too high to satisfy mission requirements.
2. High-speed flyby opportunities will be less numerous and restricted to a tighter window around the initial orbital nodes of the spacecraft with respect to the target asteroid's orbital plane.

The same assumptions can be made, but with less certainty, if T_{max} is only slightly greater than T_{min}. What constitutes a prohibitively small difference between T_{max} and T_{min} must be evaluated on a case by case basis, but can be qualitatively assessed. If it appears that extensive phasing will be required to reach the target, then a tight T_{max} and T_{min} bound is likely to result in an inability to match both the phase angle the inclination before crossing the communications barrier. The above heuristic formulation is by no means exact, but does give one a good idea of when a contingency trajectory option may be available.

4.1.1. Initial launch date analysis: October 7, 2018

Asteroid 1991 VG was initially selected as the primary target for the October 2018 launch of EM-1, and under ideal circumstances, represents the most optimal target for a mission beginning in the latter half of that year [5]. Uncontrolled propagation of NEA Scout's true ICA-state for the 2018 mission, shown in Fig. 5, results in a low inclination trajectory flowing along the Sun-Earth invariant manifolds towards 1991 VG [10–12]. The favorable departure direction bodes well for the possibility of reestablishing a constraint-satisfying trajectory for this launch date. Previous analysis, has indicated that the minimum time of flight for a rendezvous with 1991 VG is between 600 and 800 days for a nominal 2018 mission scenario [9]. This circumvents the previously described estimate of T_{min}, and roughly bounds possible solutions to between 800 and 990 days TOF.

A quick glance at Fig. 3 might suggest that 2013 BS45 is the next logical option, but the combination of its clockwise heading and location ahead of Earth in the Sun-Earth rotating frame would likely make it a difficult target for NEA Scout to reach with the given initial state. The next target listed, 2013 RZ53, appears to be a viable alternative. It possesses similar location and orbital characteristics to 1991 VG when viewed in the Sun-Earth rotating frame, albeit with a higher inclination relative to the departure trajectory. Asteroids 2007 UN12 and 2008 EA9 also represent feasible targets. As seen in Table 2, both asteroids have large upper bounds on the TOF, but the time needed to correct for the considerable initial phase angle differences could potentially push possible rendezvous towards the high end of the feasibility range.

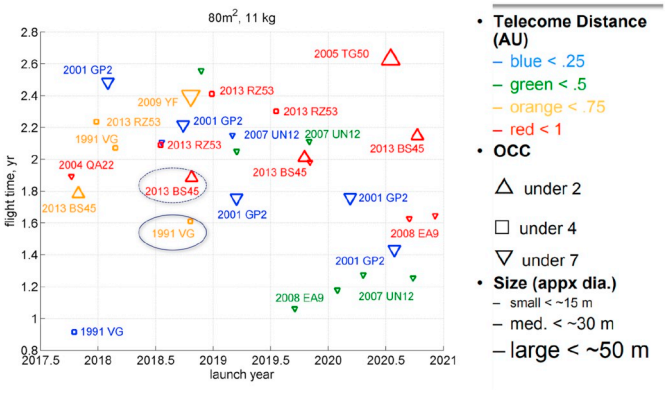

Fig. 3. Possible Target NEAs for variable launch dates [9].

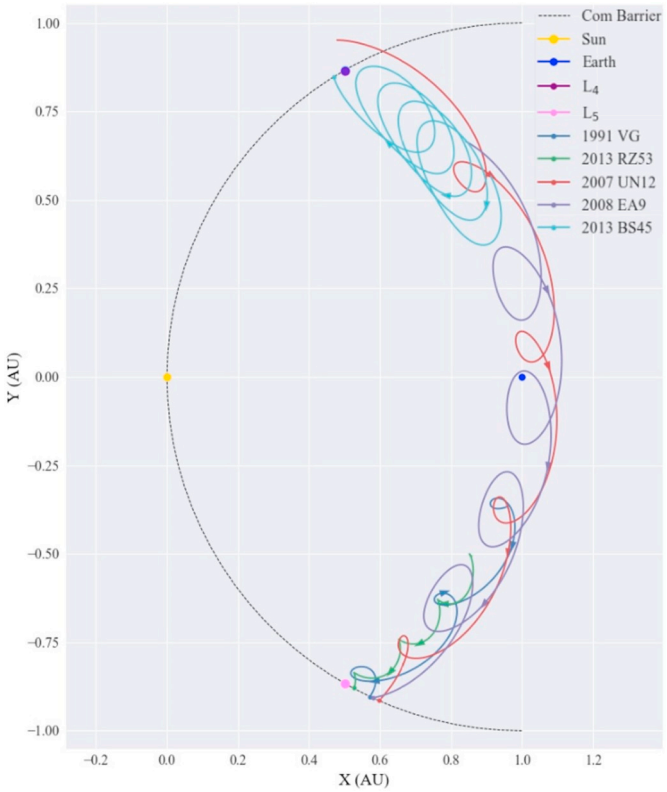

Fig. 4. Target NEA orbits from October 24, 2017 until their first crossing of the 1 AU communications barrier. (Sun-Earth rotating frame).

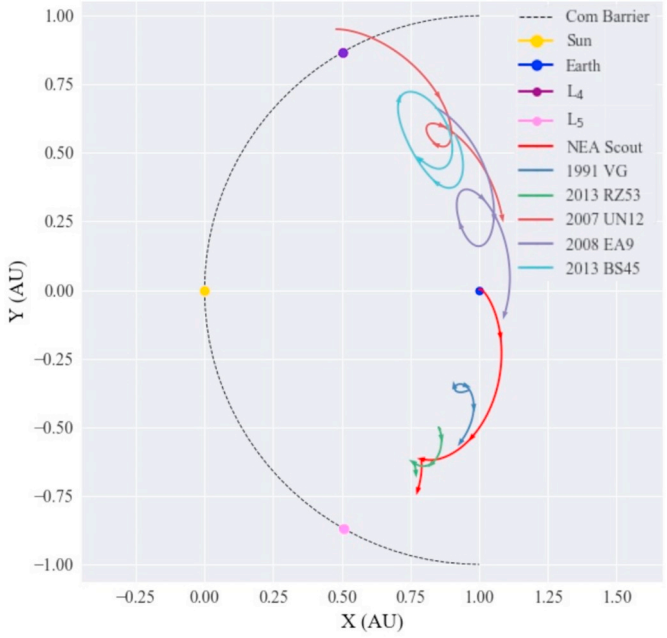

Fig. 5. 500 day propagation of NEA-Scout's ICA-state for the October 7, 2018 launch date along with potential target asteroids.

4.1.2. New launch date analysis: December 2019

The aforementioned delay of EM-1 to December of 2019 necessitates new ICA-states. A range of possible initial conditions were computed using the ICA-state from the October 2018 mission. The epoch times, therefore, can range from December 17, 2019 to January 17, 2020. Uncontrolled 75 day propagation of a subset of these initial conditions can be seen in Fig. 6(a) on the next page.

Table 2
Transfer time bounds for October 7, 2018 mission.

Target	T_{min} (days)	T_{max} (days)
1991 VG	452	995
2013 BS45	278	1683
2013 RZ53	722	1286
2007 UN12	334	1619
2008 EA9	357	1657

Lower bounds on transfer times, T_{min}, to each target vary non-linearly with the chosen launch date. The values given in Table 3 are an average over the previously mentioned time intervals. The 31 day launch window coupled with 28 day lunar cycle offer considerable control over the general direction of the departure trajectory. Based on preliminary analysis, 2007 UN12 and 2008 EA9 appear to be favorable targets for ICA-states ranging from Jan 4, 2020 to Jan 16, 2020. Fig. 6(b) and (d) highlight the location of 2007 UN12 and 2008 EA9 relative to the favorable ICA-states.

On these dates, NEA Scout departs along the Sun-Earth manifolds heading towards the Sun-Earth L_5 Lagrange point while 2008 EA9 and 2007 UN12 follow close behind. Also promising is the small plane change time (T_{min}) for NEA Scout relative to each target over the entirety of the launch month. Additionally, T_{max} for each target is on average 1200 days, providing considerable time for maneuvering. With the addition of sail control, the spacecraft can potentially rendezvous with these targets sooner than the equivalent 2018 mission.

For the remainder of the launch window, asteroid 2013 BS45 appears to be a good choice for a rendezvous target. This asteroid possesses a larger initial phase angle with respect to NEA Scout than 2007 UN12 or 2008 EA9, but retains a high upper bound on flight time. As seen in Fig. 6(c), the trajectories flow towards the Sun-Earth L_4 Lagrange point and close the existing phase angle within 800–900 days. Extensive maneuvering will be required to arrive at low speeds relative to the target asteroid, but the relatively small T_{min} will allow for NEA Scout to spend the majority of the trajectory thrusting in plane with 2013 BS45.

Asteroids 1991 VG and 2013 RZ53, however, seem to be poor targets compared to the previous launch date. In both cases, the additional 420 days has brought the T_{min} - T_{max} bounds close together, and violated the bounds in the case of 2013 RZ53. This implies that the time spent changing inclination will dominate the sail maneuvering schedule, leaving little time to overcome the now larger phase angles.

4.2. State-space model

Prior to investigating trajectories to one of the proposed targets, a discrete state-space model for the trajectory and relevant mission constraints is constructed. This is done by first defining the entire trajectory, $\vec{X}_L$, as a vector of n discrete states, $\vec{X}_i$, as illustrated below in Equation (9).

$$\vec{X}_L = [\,\vec{X}_1\,,\ \vec{X}_2\,,\ldots,\ \vec{X}_n\,];\ \vec{X}_i = \left[\ \vec{r_c}\ ,\ \dot{\vec{r_c}}\ ,\ t\ ,\ \alpha\ ,\ \gamma\ ,\right] \tag{8}$$

Vectors $\vec{r_c}$ and $\dot{\vec{r_c}}$ represent the x-y-z components of the spacecraft's position and velocity relative to the solar system's barycenter. Element t is the epoch time of the state and determines the true positions of all bodies in the ephemeris formulation for n-body gravitation and SRP. As stated earlier, cone angle, α, and clock angle, γ, orient the normal vector and thrust of the sail relative to the Sun-sail line and by geometrical transformation to the solar system's barycenter. From Equations (1) and (2), a discrete model can be expressed for the time derivative of the spacecraft's state, $\dot{\vec{X}}_i$. Equation (9) assumes that α and γ are discrete control variables, and that time, t, is linearly represented.

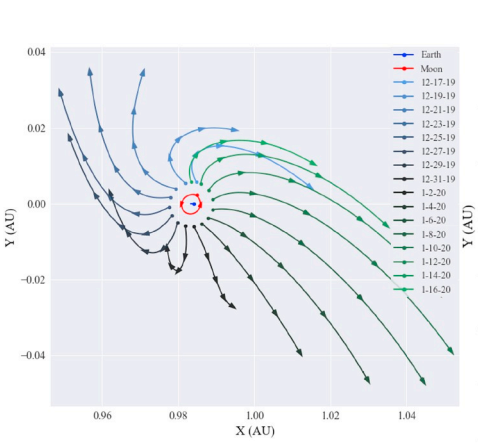

(a) ICA-state propagation for 75 days-Moon in red.

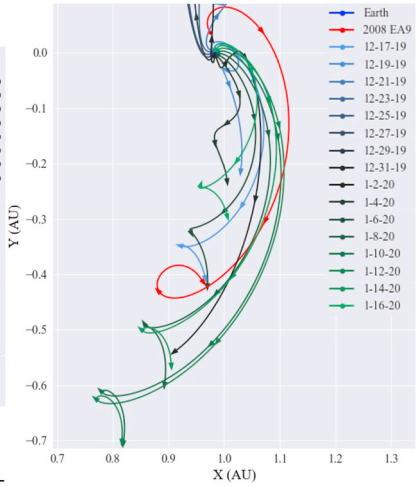

(b) ICA-state propagation for 500 days-2008 EA9 in red.

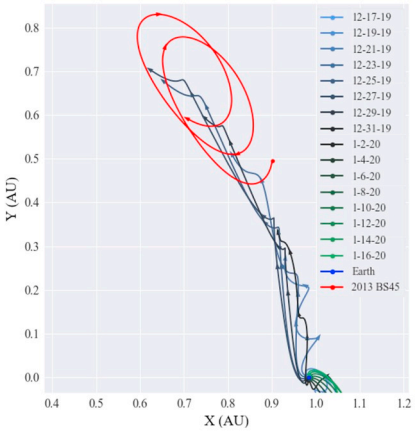

(c) ICA-state propagation for 800 days-2013 BS45 in red.

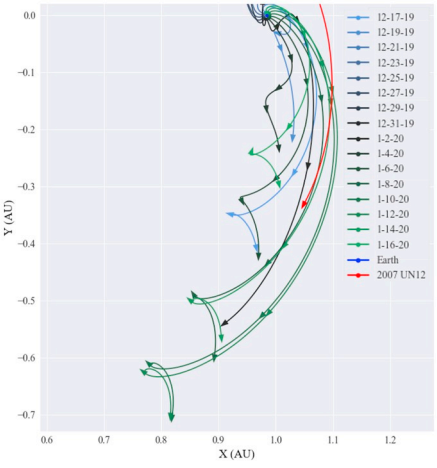

(d) ICA-state propagation for 500 days-2007 UN12 in red.

Fig. 6. Propagation of updated ICA-state vectors as viewed in the Sun-Earth rotating frame. The legend indicates the date of each initial state. The Earth and Moon are shown only from December to January.

Table 3
Average transfer time bounds for a December 2019 mission.

Target	T_{min} (days)	T_{max} (days)
1991 VG	380	575
2013 BS45	95	1263
2013 RZ53	945	866
2007 UN12	340	1199
2008 EA9	120	1237

$$\dot{\vec{X}}_i = \left[\dot{\vec{r}}_c \ , \ \ddot{\vec{r}}_c \ , \ 1 \ , \ 0 \ , \ 0 \right] \quad Where \quad \ddot{\vec{r}}_c = \ddot{\vec{r}}_{sail} + \ddot{\vec{r}}_{gravity} \tag{9}$$

Construction of a total mission constraint vector begins by first considering the boundary conditions for a successful contingency trajectory. The initial state constraint, denoted $\vec{C}_s(\vec{X}_1)$, enforces that the trajectory begins at pre-specified ICA-state dictated by the chosen launch date. Terms $C_p(\vec{X}_n, b_n^p)$ and $C_v(\vec{X}_n, b_n^v)$ represent the terminal position and velocity conditions of a low speed flyby relative to the target asteroid.

$$\vec{C}_s(\vec{X}_1) = \vec{X}_1 - \vec{X}_{ICA} = \vec{0} \quad [1\text{: } 7] \tag{10}$$

$$C_p(\vec{X}_n, b_n^p) = 2.0 \text{ km} - |\vec{r}_c - \vec{r}_{Targ}[t_n]| - |b_n^p| = 0 \tag{11}$$

$$C_v(\vec{X}_n, b_n^v) = 100 \text{ m/ s} - |\dot{\vec{r}}_c - \dot{\vec{r}}_{Targ}[t_n]| - |b_n^v| = 0 \tag{12}$$

The non-negative terms, b_n^v and b_n^p, known as slack variables, convert the original inequality constraints into equality constraints. Additional constraints must now be placed upon the cone angle, α, in each state. For each $\vec{X}_i$ this constraint can also be expressed with the aid of additional slack variables, b_i^u and b_i^l.

$$\vec{C}_\alpha(\vec{X}_i) = \begin{bmatrix} 50 - \alpha - |b_i^u| \\ \alpha - |b_i^l| \end{bmatrix} = \vec{0} \tag{13}$$

All slack variables are stored in the slack vector, $\vec{B}$, and all constraints are appended to vector, $\vec{C}(\vec{X}_L, \vec{B})$.

$$\vec{B} = [\, b_1^u \ , \ b_1^l \ , \ b_2^u \ , \ b_2^l \ , \ldots b_n^u \ , \ b_n^l \ , \ b_n^p \ , \ b_n^v] \tag{14}$$

$$\vec{C}(\vec{X}_L, \vec{B}) =$$

$$\left[\ \vec{C}_s(X_1)\ ,\ C_p(\vec{X}_n, b_n^p)\ ,\ C_v(\vec{X}_n, b_n^v)\ ,\ \vec{C}_\alpha(X_1, b_1^l, b_1^u), ..., \vec{C}_\alpha(\vec{X}_n, b_n^l, b_n^u)\ ,\right]$$

In this form, the converged solution will satisfy the constraints if the states in $\vec{X}_L$ and slacks in $\vec{B}$ satisfy $\vec{C}(\vec{X}_L, \vec{B}) = \vec{0}$.

4.3. Control law initial guess construction

To initialize the trajectory vector $\vec{X}_L$, a simplified locally-optimal control law is used to construct a partial transfer onto the target's orbit from the initial state $\vec{X}_1$. The control law, similar to that described by Petropolus and Dachwald, is formulated by converting the instantaneous state of both the sailcraft, $\vec{X}_i$, and the target asteroid, $\vec{X}_{Targ}$, into sets of five classical orbital elements describing their osculating orbits about the Sun [16–18]. A function 'Q' may then be constructed which quantifies the 'distance' between the orbit of the sail and the target. Q is the sum of the differences between each orbital element divided by the maximal rate of change possible over the current set of orbital elements [17].

$$Q = \sum_{j=1}^{5} = \left(\frac{\Delta\vec{O}\,[j]}{\Delta\dot{\vec{O}}_{max}[j]}\right)^2 \quad where \quad \Delta\vec{O} = \vec{O}_i - \vec{O}_{Targ} = \begin{bmatrix} a_i - a_{Targ} \\ e_i - e_{Targ} \\ i_i - i_{Targ} \\ \Omega_i - \Omega_{Targ} \\ \omega_i - \omega_{Targ} \end{bmatrix} \tag{15}$$

The control law chooses an α and γ to orient the solar sail in a direction that will instantaneously minimize $\dot{Q}$, the time rate of change of Q [15]. NEA Scout is then propagated under this set of sail controls in the full force model for a finite amount of time, after which the process is repeated. At each minimization of Q, the current state $\vec{X}_i$ is concatenated into the vector $\vec{X}_L$ in order to construct the initial state and control history for the spacecraft. Under ideal circumstances the control law will eventually yield a trajectory which arrives on or close to the target's osculating orbit, but not necessarily at the target object. In fact, the lack of control over the spacecraft's initial true anomaly can lead to the target and spacecraft having a large phase angle difference at the solution of Q [16,17]. For this reason, the control law is typically not run until $Q = 0$. Instead, it is terminated once the spacecraft makes a sufficiently close approach with the target. Despite these limitations, the law supplies a viable initial guess for the sail control history.

4.4. Trajectory transcription

Given an initial guess for $\vec{X}_L$, 7^{th} order Gauss Lobatto collocation is used to transcribe the equations of motion into a form suitable for efficient numerical solving and optimization. This technique is an example of the popular direct transcription class, and was first described by Hermann and Conway [19,20]. Analysis has shown the method to be more effective than other direct transcriptions in trajectory optimization problems [21]. The method constructs 7^{th} order polynomials between states $\vec{X}_i$ in the total design vector $\vec{X}_L$. The equations of motion are considered satisfied if the resulting time-derivative of this piecewise polynomial matches that of the underlying system dynamics at predefined 'collocation' points [22]. These polynomials along with the mission constraints, $\vec{C}(\vec{X}_L, \vec{B})$ can be solved for simultaneously to yield a feasible trajectory.

For a single 7^{th} order Lobatto polynomial arc, 4 successive 'node' states $\vec{X}_1^N$ through $\vec{X}_4^N$ in $\vec{X}_L$ are necessary (superscript N is applied for clarity) [21,23–25]. The unique 7^{th} order polynomial is then constructed and evaluated at the three interior collocation points. This entire process can be summarized in a common Equation (16) for the i^{th} collocation point.

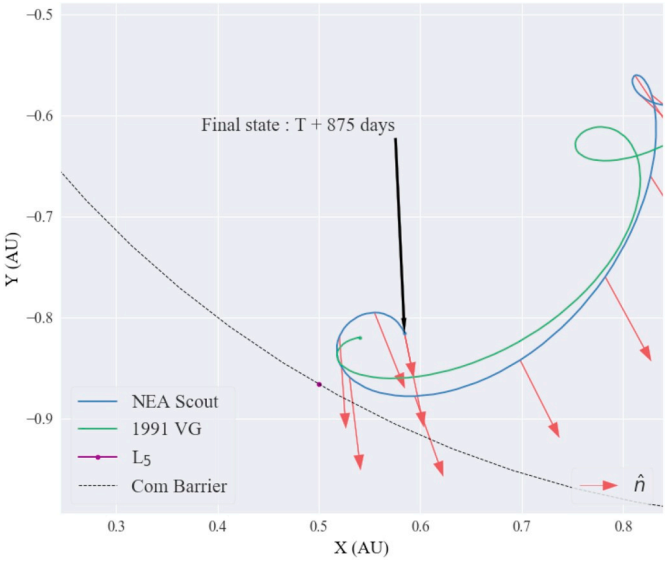

Fig. 7. Position of NEA Scout and 1991 VG after 875 days of control law propagation.

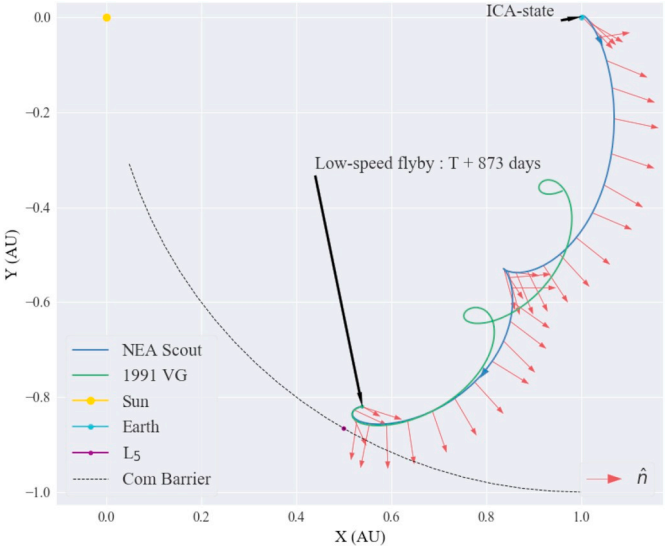

Fig. 8. A low-speed flyby with 1991 VG viewed in the Sun-Earth rotating frame. The red arrows indicate the direction of the sail normal vector, $\hat{n}$. (For interpretation of the references to color in this figure legend, the reader is referred to the Web version of this article.)

Table 4
Sample early flyby trajectories of 1991 VG for the October 7, 2018 mission.

TOF(days)	Flyby Distance (km)	Flyby Speed (km/s)
263	1.83	1.43
441	0.57	1.06
611	2.21	0.65
716	1.33	0.16

$$\vec{X}_i^C\,[1\colon 6] = \left(a_1^i\vec{X}_1^N + a_2^i\vec{X}_2^N + a_3^i\vec{X}_3^N + a_4^i\vec{X}_4^N + \Delta t\left(b_1^i\dot{\vec{X}}_1^N + b_2^i\dot{\vec{X}}_2^N + b_3^i\dot{\vec{X}}_3^N + b_4^i\dot{\vec{X}}_4^N\right)\right)[1\colon 6]$$
$$\vec{X}_i^C\,[7] = \vec{X}_1^N\,[7] + \tau_i\Delta t \tag{16}$$

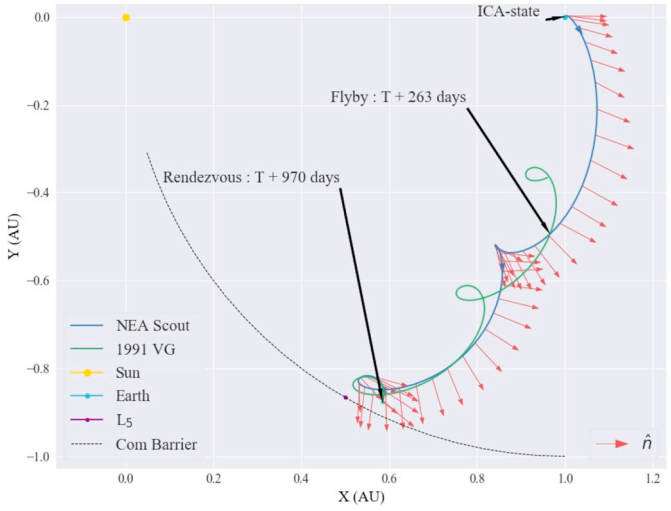

Fig. 9. A high speed flyby of 1991 VG at T + 263 days to rendezvous at T + 970 days.

$$\vec{X}_i^C[8{:}\,9] = \overrightarrow{X_i^N}[8{:}\,9]$$

The node state spacings, τ_i, along with the coefficients, a_j^i and b_j^i shown above, are unique to 7^{th} order Gauss Lobatto collocation, and their precise values can be found in the referenced works of Grebow and Ozimek [24,25]. Sail angles α and γ at the i^{th} collocation point are assumed to be piecewise constant and inherited from the i^{th} node state. In this formulation, the total arc time is free to move by varying the epoch times at the first and last node states. The 'defect' equation, $\vec{\delta}_i$, representing the difference between the polynomial derivatives and the true derivatives at each of the three collocation points then takes the common form of Equation (17),

$$\vec{\delta}_i = \left(e_1^i\vec{X}_1^N + e_2^i\vec{X}_2^N + e_3^i\vec{X}_3^N + e_4^i\vec{X}_4^N + \Delta t\left(f_1^i\dot{\vec{X}}_1^N + f_2^i\dot{\vec{X}}_2^N + f_3^i\dot{\vec{X}}_3^N + f_4^i\dot{\vec{X}}_4^N + f_5^i\dot{\vec{X}}_i^C\right)\right)[1{:}\,6] = \vec{0} \tag{17}$$

where e_j^i and f_j^i are additional coefficients associated with the 7^{th} order Gauss Lobatto method. The full constraint equation to be satisfied for a single Gauss Lobatto arc can be seen in Equation (18).

$$\vec{F}\left(\vec{X}_1^N, \vec{X}_2^N, \vec{X}_3^N, \vec{X}_4^N\right) = \left[\vec{\delta}_1, \vec{\delta}_2, \vec{\delta}_3\right] = \vec{0} \tag{18}$$

Table 5
Additional sample low speed flyby trajectories for the October 7, 2018 mission.

Target	TOF (days)	Flyby Distance (km)	Flyby Speed (m/s)
1991 VG	880	0.6	2.3
2013 RZ53	1056	1.5	15.5
2007 UN12	1353	0.9	63.2
2008 EA9	1316	0.3	74.5

Additional constraints, which have been omitted for brevity, are employed to strictly enforce both the forward direction of time, and the correct time spacing of the two interior node states on the normalized time interval between $\vec{X}_1^N$ and $\vec{X}_4^N$.

An entire piecewise representation of the trajectory is created by linking each Lobatto arc together at the first and last node state. The defect equations for each arc can be added, along with the mission constraints, into a single vector $\vec{F}(\vec{X}_L, \vec{B})$ shown in Equation (19).

$$\vec{F}(\vec{X}_L, \vec{B}) = \begin{bmatrix} \vec{F}(\vec{X}_1, \vec{X}_2, \vec{X}_3, \vec{X}_4) \\ \vec{F}(\vec{X}_4, \vec{X}_5, \vec{X}_6, \vec{X}_7) \\ \vdots \\ \vec{F}(\vec{X}_{3m-2}, \vec{X}_{3m-1}, \vec{X}_{3m}, \vec{X}_{3m+1}) \\ \vec{C}(\vec{X}_L, \vec{B}) \end{bmatrix} \tag{19}$$

For a trajectory consisting of m Lobatto arcs, the number of states, n, must obey $n = (3m + 1)$. As an additional error check, collocation solutions are also verified with a multiple shooting algorithm. Each $\vec{X}_i$ is explicitly integrated to the epoch time of $\vec{X}_{i+1}$ in the trajectory vector, $\vec{X}_L$. To satisfy the system dynamics, the trajectory must be continuous in both position and velocity between states. This can be expressed via Equation (20) where $\overrightarrow{X_i}(t_{i+1})$ represents the integration of the i^{th} state to the epoch time of $\vec{X}_{i+1}$. Equation (20) then replaces the defect equations in $\vec{F}(\vec{X}_L, \vec{B})$.

$$\vec{F}(\vec{X}_i, \vec{X}_{i+1}) = (\overrightarrow{X_i}(t_{i+1}) - \vec{X}_{i+1})[1{:}\,6] \tag{20}$$

The independence of each arc helps to distribute any error remaining in a solution throughout the entire trajectory. Similar to collocation, TOF is allowed to vary by choosing the epoch time of the individual states. Likewise, sail angles α and γ are assumed piecewise constant along the i^{th} arc and inherited from Refs. $\vec{X}_i$[10,12]. The multiple shooting scheme is accurate to the tolerances of the underlying integration method, therefore its convergence assures the accuracy of the solution.

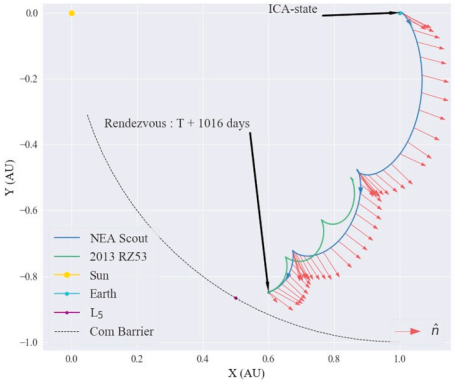

(a) 2013 RZ53 rendezvous trajectory.

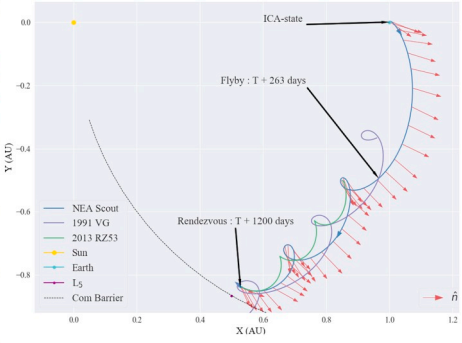

(b) A 1991 VG flyby to 2013 RZ53 rendezvous trajectory.

Fig. 10. 2013 RZ53 trajectory options.

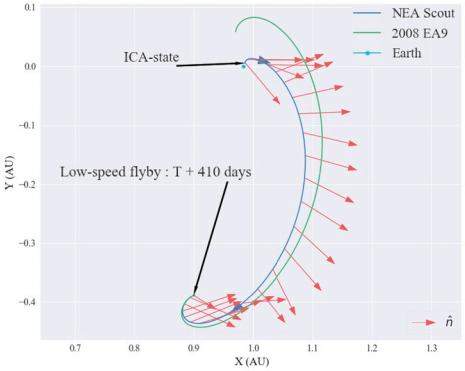

(a) A 410 day TOF low-speed flyby trajectory (73 m/s) to 2008 EA9. The ICA-state occurs on January 9, 2020 corresponding to a launch date of December 22, 2019.

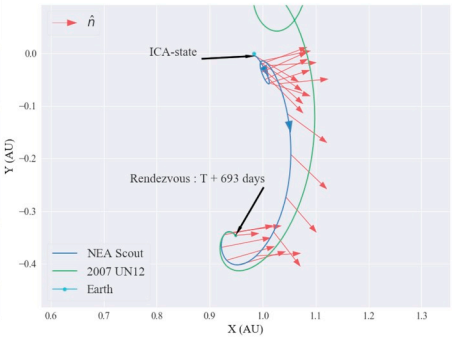

(b) A 693 day TOF rendezvous trajectory with 2007 UN12. The ICA-state occurs on January 5, 2020 corresponding to a launch date of December 19, 2019.

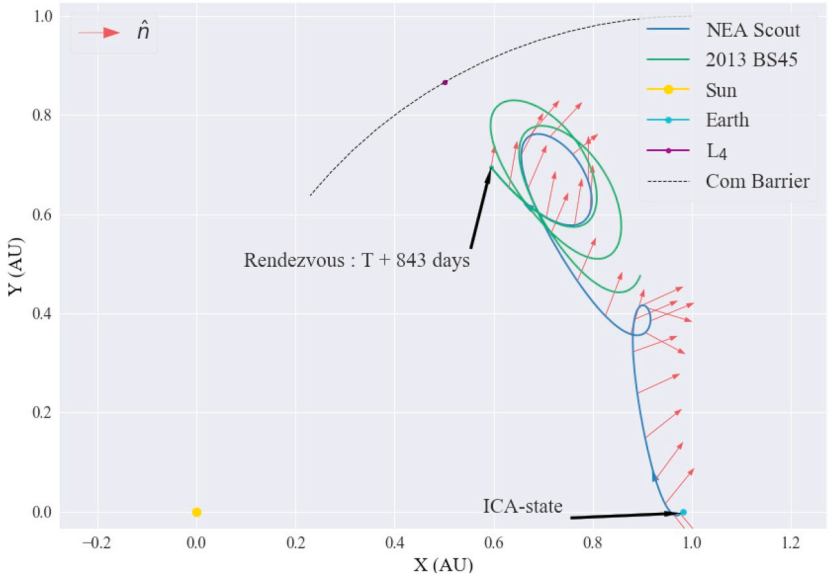

(c) An 843 day TOF rendezvous trajectory with 2013 BS45. The ICA-state occurs on December 27, 2020 corresponding to a launch date of December 10, 2019.

Fig. 11. Sample trajectories to 2007 UN12, 2008 EA9, and 2013 BS45.

Table 6
Additional sample of low speed flyby trajectories for December 2019.

Target	Launch Date	TOF(days)	Flyby Distance (km)	Flyby Speed (m/s)
2013 BS45	12-10-19	815	1.41	86.2
2008 EA9	12-29-19	415	0.15	79.7
2007 UN12	12-21-19	685	0.56	94.4

4.5. Trajectory targeting

In aerospace trajectory design, directly solving $\vec{F}(\vec{X_L}, \vec{B})$ is often referred to as targeting. In this case, regardless of whether collocation or multiple shooting is used, the targeting problem is a large non-linear system of equations consisting of several thousand constraints and independent variables. This must be solved via an iterative Newton-type method. Given an initial guess for $\vec{X}_{L\,i}$, Newton's method takes the form of Equation (21) [11,12,24–26].

$$\begin{bmatrix} \vec{X}_{L\,i+1} \\ \vec{B}_{i+1} \end{bmatrix} = \begin{bmatrix} \vec{X}_{L\,i} \\ \vec{B}_{i} \end{bmatrix} - D\vec{F}(\vec{X}_{L\,i}, \vec{B}_i)^T \left(D\vec{F}(\vec{X}_{L\,i}, \vec{B}_i)\, D\vec{F}(\vec{X}_{L\,i}, \vec{B}_i)^T \right)^{-1} \vec{F}(\vec{X}_{L\,i}, \vec{B}_i) \tag{21}$$

Term $D\vec{F}(\vec{X_L}, \vec{B})$ is the Jacobian matrix consisting of the partial derivatives of $\vec{F}(\vec{X_L}, \vec{B})$ with respect to each variable in $\vec{X_L}$ and $\vec{B}$. The Jacobian computed at each iteration typically contains over 1 million elements. Fortunately, the discretization of the trajectory into independent Lobbatto or shooting arcs results in a sparse problem where

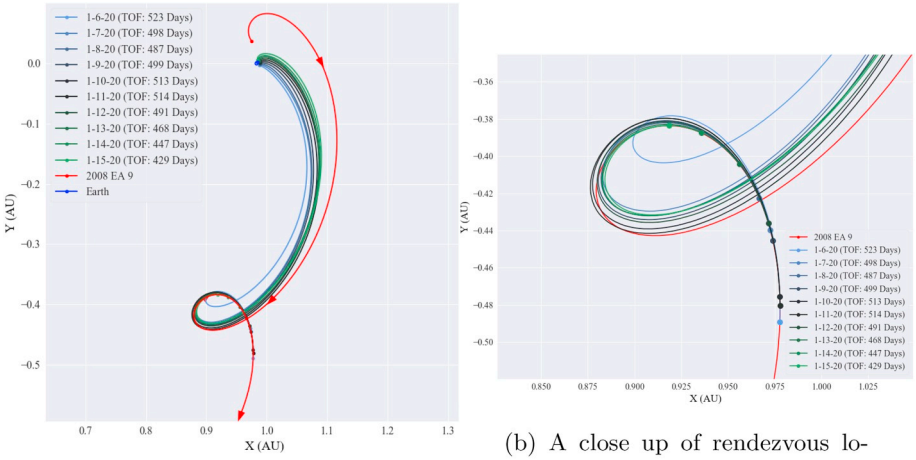

(a) An overall view of the trajectory family towards asteroid 2008 EA9.

(b) A close up of rendezvous locations between NEA Scout and 2008 EA9.

Fig. 12. A family of rendezvous trajectories to asteroid 2008 EA9. The single parameter continuation scheme in the ICA-state epoch time began at 1-6-20 and progressed in 6 h increments until 1-15-20.

at least 99% of Jacobian entries are equal to zero. These can be ignored when computing $D\vec{F}(\vec{X_L}, \vec{B})$. High performance linear-algebra libraries are used to solve the sparse linear system in Equation (21) [23].

In most cases, the initial $\vec{X_L}$ provided by the control law is sufficient to allow for solution to $\vec{F}(\vec{X_L}, \vec{B})$. If not, the algorithm may not converge, necessitating either another guess for $\vec{X_L}$ from the control law, or attempting to solve a 'relaxed' version of $\vec{F}(\vec{X_L}, \vec{B})$. One common relaxation employed in this situation is raising the maximum flyby velocity restriction appended to the end of $\vec{F}(\vec{X_L}, \vec{B})$ until a solution can be found.

$$C_v(\vec{X_n}, b_n^v) = (100 + V_{relax})\ \text{m/ s} - |\dot{\vec{r}_n} - \dot{\vec{r}}_{Targ}(t_n)| - |b_n^v| = 0 \tag{22}$$

The scalar V_{relax} is the amount by which the flyby velocity restriction will be increased. The solution to this relaxed problem can then be used as a new guess to the original problem.

4.6. Trajectory optimization

Once a set of feasible solutions has been found, it is critical to search for optimal trajectories that minimize total mission cost compared to the baseline. Since a solar sail spacecraft expends no fuel for propulsion, one of the most relevant cost metrics to minimize in pursuit of this goal is the total time of flight (TOF). This optimization problem is formally stated below.

$$\textit{Minimize}: \quad T(\vec{X_L}) = \sum_{i=1}^{n-1} (\vec{X}_{i+1}[7] - \vec{X}_i[7])^2$$
$$\textit{Subject to}: \vec{F}(\vec{X_L}, \vec{B}) = \begin{bmatrix} \vec{F}(\vec{X}_1, \vec{X}_2, \vec{X}_3, \vec{X}_4) \\ \vec{F}(\vec{X}_4, \vec{X}_5, \vec{X}_6, \vec{X}_7) \\ \vdots \\ \vec{F}(\vec{X}_{n-3}, \vec{X}_{n-2}, \vec{X}_{n-1}, \vec{X}_n) \\ \vec{C}(\vec{X_L}, \vec{B}) \end{bmatrix} = \vec{0} \tag{23}$$

The cost function $T(\vec{X_L})$ is the sum of the differences in the epoch time of each successive state in the design vector squared. Defining the TOF cost in this manner allows for contribution from every state in the design vector, and helps restrict non-feasible solutions. Term $\vec{F}(\vec{X_L}, \vec{B})$ represents the dynamical and mission constraints outlined previously. Similar formulations are also used to minimize both flyby distance and velocity when required.

Local optimization of a cost function is performed via Sequential Quadratic Programming (SQP) which successively minimizes a quadratic model of the objective function, $T(\vec{X_L})$, subject to a linearization of the non-linear constraints $\vec{F}(\vec{X_L}, \vec{B})$[27,28]. As with targeting, optimization of a trajectory is initially performed with a collocation transcription and refined with multiple shooting once a solution has been found. By providing a feasible initial guess for $\vec{X_L}$, SQP will generally return a lower cost trajectory, however, there is no guarantee that this solution will be globally optimal. Unfortunately, trajectory optimization problems have many strong local minimums and saddle points which prevent convergence to the true global optimum. Attempts to mitigate this issue are made by starting the algorithm from many different initial trajectory guesses and directly targeting lower cost solutions when perceived local minima are encountered.

5. Results

5.1. Initial launch date results: October 7, 2018

The most pressing issue to be addressed for the October 2018 launch date was the viability of the primary mission to 1991 VG. Initial propagation using the control law suggested that a low-speed flyby or rendezvous was possible in the 800–990 day feasibility range.

One such run for 875 days is depicted in Fig. 7. The Q law was not able to arrive precisely at 1991 VG, but was able to reduce both the phase angle and target separation at 875 days as compared to uncontrolled propagation. The initial guesses for the trajectory vector $\vec{X_L}$ were then provided to a collocation targeter configured to find a flyby trajectory (free velocity restriction). The high convergence radius of the algorithm yielded quick solutions even when provided with poor initial guesses. At this stage of the process, flyby speeds of (200–700) m/s were typical at TOFs of 800–1100 days. An SQP minimization algorithm with a terminal flyby velocity cost function was then used to lower the flyby speed until the 100 m/s requirement was met (see Fig. 8).

These solutions were passed to another SQP algorithm configured to minimize the TOF along with the slacked flyby velocity constraint to keep new solutions bounded below the 100 m/s requirement. Once a

local minimum for the TOF was reached, the trajectories were re-converged and optimized under the same cost function and constraints using a refined collocation mesh and multiple shooting.

The process was successful in bringing the flyby speed to 80 m/s and minimizing the TOF to 873 days. Although the algorithm consistently yielded final solutions at this TOF, it is not guaranteed that this is a globally optimal solution for the given ICA-state.

As expected, the TOF of a low-speed flyby of 1991 VG appears to have increased considerably compared to a nominal trajectory (873 vs 800 days). To achieve full rendezvous (0 m/s relative velocity), an additional 7 days of transfer time is necessary. Additionally, the collocation and shooting targeting scheme was configured to search for high speed flybys over a TOF range of 200–1000 days. A sample of converged trajectories and their corresponding flyby speeds can be found in Table 4. Of particular interest and possible utility is the solution corresponding to a TOF of 263 days. It was identified upon finding that nearly all converged trajectories in 800–1100 day TOF range also made close approaches within 5 million kilometers during this time. This indicated that double flyby opportunity might be available.

Extensive targeting and local optimization were used to compute a range of flybys over this time period. The final flyby velocity of 1.43 km/s still greatly exceeds that required for the full mission success criteria as outlined in section 2, but could be sufficient to achieve partial target characterization early in the mission. Mission operators would have the choice to continue on to a second flyby/rendezvous with 1991 VG, or to divert to another target NEA. Such a maneuver could be necessary in the (highly) unlikely event that 1991 VG were discovered to be a spent Saturn 5 upper stage as some have speculated in the past [29]. The combination of this flyby with a return to rendezvous with 1991 VG at T + 970 days is depicted in Fig. 9. Note that the spacecraft is still within the communications range.

Once the major questions regarding 1991 VG were addressed, work was directed at evaluating the other feasible targets in the design space outlined in section 4. The most promising of these candidates was asteroid 2013 RZ53. The same targeting sequence was applied in order to converge mission operable trajectories. One rendezvous solution with a TOF of 1016 days is depicted in Fig. 10(a). The additional transfer time of 150 days can be attributed to 2013 RZ53's higher inclination relative to NEA Scout's initial orbit (T_{min} = 722 days), necessitating large amounts of time thrusting out of plane. Since 2013 RZ53 was still 250 days away from its T_{max}, it was possible to exploit the aforementioned early flyby of 1991 VG. A two phase trajectory combining the same early flyby of 1991 VG followed by a rendezvous with 2013 RZ53 at 1200 days can be seen in Fig. 10(b). This trajectory could present a good alternative option should mission operators wish to divert from a rendezvous with 1991 following the initial encounter. Trajectories to the remaining asteroids that were surveyed (2007 UN12, 2008 EA9) required considerably longer mission times in order to satisfy all mission constraints (see Table 5). While all of the relevant mission requirements are met, it would be difficult to justify the additional 300 days TOF as compared to a 1991 VG or 2013 RZ53 trajectory.

5.2. New launch date results: December 2019

Work thus far has shown asteroid 2008 EA9 to be a desirable target in terms of TOF and communications distance for the December 2019 mission. A low TOF trajectory to 2008 EA9 is illustrated in Fig. 11(a) on the next page. It assumes an EM-1 launch date of December 22, 2019 and enables NEA Scout to perform a low-speed flyby (73 m/s) in just 410 days. The short transfer time is due to the small phase angle between NEA Scout and the target at the outset of the contingency scenario as well as the θ_i of 0.28 deg. This allows NEA Scout to spend the majority of the time phasing with the target rather than matching inclinations. One can note the importance of an optimal departure trajectory by comparing the rendezvous time with 2008 EA9 in 2019 with that in 2018. The TOF, plus the additional time between launch dates, is still less than that of the equivalent 2018 mission.

The second best asteroid target in terms of TOF and communications distance was identified as 2007 UN12. A rendezvous trajectory with a launch date of December 19, 2019 and TOF of 693 days can be seen in Fig. 11(b) on the next page. This particular solution, has NEA Scout loiter in close proximity of the Earth while matching target inclinations. The spacecraft then departs for 2007 UN12 once it has crossed below Earth's position as viewed in the Sun-Earth rotating frame. While TOF is still considerably smaller than any option from the October 2018 mission, the 300 day loop implies that the optimal launch date is likely roughly 300 days in the future. This could make 2007 UN12 an attractive low TOF target should EM-1 be delayed into 2020.

Asteroid 2013 BS45 was the third best option based off of the aforementioned metrics. A typical rendezvous trajectory with a TOF of 843 days is shown in Fig. 11(c) on the next page. The departure trajectory results in a θ_i of 0.06°, meaning that NEA Scout can spend the majority of the trajectory thrusting in plane to phase with the target. Despite the higher TOF, 2013 BS45 presents a unique option compared to the previously mentioned targets. The asteroid is flowing away from Earth and towards the Sun-Earth L_4 Lagrange point. In fact, the nominal orbit of 2013 BS45 seems similar to that of an L_4 periodic orbit at the time of its crossing of the 1 AU communications barrier [11,12]. The converged trajectory can be leveraged to insert the spacecraft into an orbit about L_4 after a successful flyby of 2013 BS45. An assessment of the feasibility and utility of this option will be the subject of future investigations.

Additional sample trajectory options with varying launch dates, flyby speeds, and target asteriods may be seen in Table 6. Attempts were also made to compute trajectories to 1991 VG and 2013 RZ53, but so far no constraint satisfying solutions have been found for the December 2019 launch window in the case of trim maneuver failure. As expected, the one year launch delay seems to have placed both asteroids too far out of range. NEA Scout is unable to rendezvous with either target before it crosses the 1 AU communication distance barrier.

The exact launch date of EM-1 in December of 2019 has not yet been determined, and once defined, could still be subject to local launch delays. Therefore, it is prudent to establish contingency options for a range of possible launch dates over the launch window. One such set of solutions for 2008 EA9 can be seen in Fig. 12. As was evident from Fig. 6, launch dates between December 20 and 31 resulted in departure trajectories that seemed favorable to this target. A family of rendezvous trajectories to 2008 EA9 were then computed over this date-range via single parameter continuation in ICA-state epoch time. TOF varies considerably, but remains within a readily acceptable 430–530 day range. These times are subject to improvement with further optimization. Similar trajectory families can also be constructed for the launch dates conducive to missions to 2013 BS45 and 2007 UN12.

In the future, once a concrete launch date and nominal trajectory have been defined, it will be possible to re-evaluate trajectory options under the same constrained circumstances as the previous October 7, 2018 mission. If the mission profile remains consistent, the preliminary solutions found above will provide an excellent starting point for a more thorough analysis.

6. Conclusion and future work

The work presented in this study suggests that even with the failed trim maneuver and lunar flyby, the NEA Scout mission is still capable of achieving its primary goals. Solar sail trajectories to initial target asteroid, 1991 VG, and alternative targets were designed, optimized, and assessed based on the initial conditions from the previously defined launch date of October 7, 2018. Rendezvous with the primary target, 1991 VG, still represented the most optimal mission profile in terms of TOF, however, with the change in launch date, low-speed flyby is uncertain. Alternatively, trajectories to other NEAs presented feasible

solutions that can potentially replace or augment the baseline contingency trajectory. Initial work was also performed to update this study for EM-1's new tentative December 2019 launch date. Asteroids 2013 BS45, 2008 EA9, and 2007 UN12 were identified as promising targets for missions beginning in the second half of December 2019. Multiple rendezvous trajectories were computed to each target asteroid for varying launch dates. The investigation presented in this paper shows that the December 2019 launch scenario provides NEA Scout with numerous alternate NEAs and potential contingency options. Additional work, in collaboration with Marshall Space Flight Center, will be carried out to verify NEA Scout trajectory solutions for specific launch dates and the next target asteroid.

Acknowledgments

All work was performed using facilities, equipment, and software provided or created by the University of Alabama's Astrodynamics and Space Research Laboratory.

Appendix A. Supplementary data

Supplementary data to this article can be found online at https://doi.org/10.1016/j.actaastro.2019.03.050.

References

[1] O. Mori, World's first demonstration of solar power sailing by ikaros, Proceedings of 2nd International Symposium on Solar Sailing, 2010, 2010.
[2] L. Johnson, M. Whorton, A. Heaton, R. Pinson, G. Laue, C. Adams, Nanosail-d: a solar sail demonstration mission, Acta Astronaut. 68 (5–6) (2011) 571–575 https://doi.org/10.1016/j.actaastro.2010.02.008.
[3] J. Davis, Lightsail Test Mission Declared Success; First Image Complete, the planetary society, 2015.
[4] L. Johnson, L. McNutt, J. Castillo-Rogez, Near earth asteroid (NEA) Scout mission, 4th International Symposium on Solar Sailing (ISSS 2017), Kyoto, Japan, 2017.
[5] L. McNutt, L. Johnson, P. Kahn, J. Castillo-Rogez, A. Frick, Near-earth asteroid (NEA) Scout, AIAA SPACE 2014 Conference and Exposition, San Diego, CA, 2014, p. 4435.
[6] A. Heaton, K. Miller, N. Ahmad, Near earth asteroid Scout solar sail thrust and torque model, 4th International Symposium on Solar Sailing (ISSS 2017), Kyoto, Japan, 2017 https://ntrs.nasa.gov/search.jsp?R=20170001502.
[7] A.R. Sobey, T.R. Lockett, Design and development of NEA Scout solar sail deployer mechanism, 43rd Aerospace Mechanisms Symposium, Santa Clara, CA, 2016, pp. 315–328.
[8] J. Orphee, B. Diedrich, B. Stiltner, C. Becker, A. Heaton, Solar sail attitude control system for the NASA near earth asteroid Scout mission, 4th International Symposium on Solar Sailing (ISSS 2017), Kyoto, Japan, 2017.
[9] G. Carlisle, D. Landau, D. Grebow, G. Lantoine, S. Nandi, E. Gustafson, E. Riedel, F. Laipert, J. Stuart, Concurrent Mission Design of NEA Scout and Lunar Flashlight, Solar Sail CubeSat Missions, http://hdl.handle.net/2014/45823.
[10] R. Sood, K. Howell, L4, L5 solar sail transfers and trajectory design: solar observations and potential earth trojan exploration, 26th AAS/AIAA Space Flight Mechanics Meeting, vol. 158, 2016.
[11] R. Sood, Significance of Specific Force Models in Two Applications: Solar Sails to Sun-Earth L4/L5 and Grail Data Analysis Suggesting Lava Tubes and Buried Craters on the Moon, Ph.D. thesis School of Aeronautics and Astronautics, Purdue University, West Lafayette, Indiana, 5 2016.
[12] R. Sood, K. Howell, Solar sail transfers and trajectory design to sun-earth L4, L5: solar observations and potential earth trojan exploration, J. Astronaut. Sci. (2019) 1–35, https://doi.org/10.1007/s40295-018-00141-4.
[13] B. Wie, Space Vehicle Guidance, Control, and Astrodynamics, American Institute of Aeronautics and Astronautics, 2015, https://doi.org/10.2514/4.102752.
[14] G. Mengali, A.A. Quarta, Solar sail near-optimal circular transfers with plane change, J. Guid. Control Dyn. 32 (2) (2009) 456–463 https://doi.org/10.2514/1.38079.
[15] F. Abd El-Salam, Some new locally optimal control laws for sailcraft dynamics in heliocentric orbits, J. Appl. Math, vol. 2013, Hindawi Publishing Corporation, 2013, pp. 1–16 https://doi.org/10.1155/2013/353056.
[16] M. Macdonald, C.R. McInnes, Analytical control laws for planet-centered solar sailing, J. Guid. Control Dyn. 28 (5) (2005) 1038 https://doi.org/10.2514/1.11400.
[17] A.E. Petropoulos, Simple control laws for low-thrust orbit transfers, 2003 AAS/AIAA Astrodynamics Specialist Conference, Big Sky, Montana, 2003.
[18] B. Dachwald, Low-thrust Trajectory Optimization and Interplanetary Mission Analysis Using Evolutionary Neurocontrol, Ph.D. thesis, Doctoral thesis Universität der Bundeswehr München Fakultät für Luft-und Raumfahrttechnik, 2004.
[19] A.L. Herman, B.A. Conway, Direct optimization using collocation based on high-order Gauss-Lobatto quadrature rules, J. Guid. Control Dyn. 19 (3) (1996) 592–599 https://doi.org/10.2514/3.21662.
[20] F. Topputo, C. Zhang, Survey of direct transcription for low-thrust space trajectory optimization with applications, Abstract and Applied Analysis, vol. 2014, Hindawi Publishing Corporation, 2014, https://doi.org/10.1155/2014/851720.
[21] M.T. Ozimek, D.J. Grebow, K.C. Howell, A collocation approach for computing solar sail lunar pole-sitter orbits, Open Aero. Eng. J. 3 (2010) 65–75.
[22] G. Wawrzyniak, K.C. Howell, Numerical methods to generate solar sail trajectories, 2nd International Symposium on Solar Sailing, New York City College of Technology, City University of New York, Brooklyn, New York), 2010, pp. 195–200.
[23] D.J. Grebow, M.T. Ozimek, K.C. Howell, Design of optimal low-thrust lunar pole-sitter missions, J. Astronaut. Sci. 58 (1) (2011) 55–79 https://doi.org/10.1007/BF03321159.
[24] M.T. Ozimek, Low-thrust Trajectory Design and Optimization of Lunar South Pole Coverage Missions, Ph.D. thesis School of Aeronautics and Astronautics, Purdue University, West Lafayette, Indiana, 5 2010.
[25] D.J. Grebow, Trajectory Design in the Earth-Moon System and Lunar South Pole Coverage, Ph.D. thesis School of Aeronautics and Astronautics, Purdue University, West Lafayette, Indiana, 5 2010.
[26] J.T. Betts, Survey of numerical methods for trajectory optimization, J. Guid. Control Dyn. 21 (2) (1998) 193–207 https://doi.org/10.2514/2.4231.
[27] A. Barclay, P.E. Gill, J.B. Rosen, SQP Methods and Their Application to Numerical Optimal Control, Variational Calculus, Optimal Control and Applications, (1998), pp. 207–222.
[28] P.E. Gill, W. Murray, M.A. Saunders, SNOPT: an SQP algorithm for large-scale constrained optimization, SIAM Rev. 47 (1) (2005) 99–131 https://doi.org/10.1137/S0036144504446096.
[29] C. de la Fuente Marcos, R. de la Fuente Marcos, Dynamical evolution of near-Earth asteroid 1991 VG, Mon. Not. Roy. Astron. Soc. 473 (3) (2017) 2939–2948 https://doi.org/10.1093/mnras/stx2545.